HHS Public Access

Author manuscript

Acta Biomater. Author manuscript; available in PMC 2018 July 15.

Published in final edited form as:

Acta Biomater. 2017 July 15; 57: 251–261. doi:10.1016/j.actbio.2017.04.023.

Folic Acid-Decorated Polyamidoamine Dendrimer Exhibits High Tumor Uptake and Sustained Highly Localized Retention in Solid Tumors: Its Utility for Local siRNA Delivery

Leyuan Xu[1,2,#], **W. Andrew Yeudall**[3,4], and **Hu Yang**[1,5,6,*]

[1]Department of Chemical and Life Science Engineering, Virginia Commonwealth University, Richmond, Virginia 23219

[2]Department of Biomedical Engineering, Virginia Commonwealth University, Richmond, Virginia 23284

[3]Department of Oral Biology, Augusta University, Augusta, Georgia 30912

[4]Molecular Oncology and Biomarkers Program, Georgia Cancer Center, Augusta University, Augusta, Georgia 30912

[5]Department of Pharmaceutics, Virginia Commonwealth University, Richmond, Virginia 23298

[6]Massey Cancer Center; Virginia Commonwealth University, Richmond, Virginia 23298

Abstract

The utility of folic acid (FA)-decorated polyamidoamine dendrimer G4 (G4-FA) as a vector was investigated for local delivery of siRNA. In a xenograft HN12 (or HN12-YFP) tumor mouse model of head and neck squamous cell carcinomas (HNSCC), intratumorally (i.t.) injected G4-FA exhibited high tumor uptake and sustained highly localized retention in the tumors according to near infrared (NIR) imaging assessment. siRNA against vascular endothelial growth factor A (siVEGFA) was chosen as a therapeutic modality. Compared to the nontherapeutic treatment groups (PBS solution or dendrimer complexed with nontherapeutic green fluorescent protein siRNA [siGFP]), G4-FA/siVEGFA showed tumor inhibition effects in single-dose and two-dose regimen studies. In particular, two doses of G4-FA/siVEGFA i.t. administered eight days apart resulted in a more profound inhibition of tumor growth, accompanied with significant reduction in angiogenesis, as judged by CD31 staining and microvessel counts. Tumor size reduction in the two-dose regimen study was ascertained semi-quantitatively by live fluorescence imaging of YFP tumors and independently supported antitumor effects of G4-FA/siVEGFA. Taken together, G4-FA

*Correspondence should be addressed to Hu Yang, Department of Chemical and Life Science Engineering, Virginia Commonwealth University, 737 North 5th Street, Biotech Eight, Richmond, VA 23219, USA. Tel.: 1-804-828-5459; Fax: 1-804-828-4454; hyang2@vcu.edu.

#Current address: Department of Internal Medicine, Yale University, New Haven, Connecticut 06520

Disclosures

The authors do not have any conflicts of interest.

shows high tumor uptake and sustained retention properties, making it a suitable platform for local delivery of siRNAs to treat cancers that are readily accessible such as HNSCC.

Graphical abstract

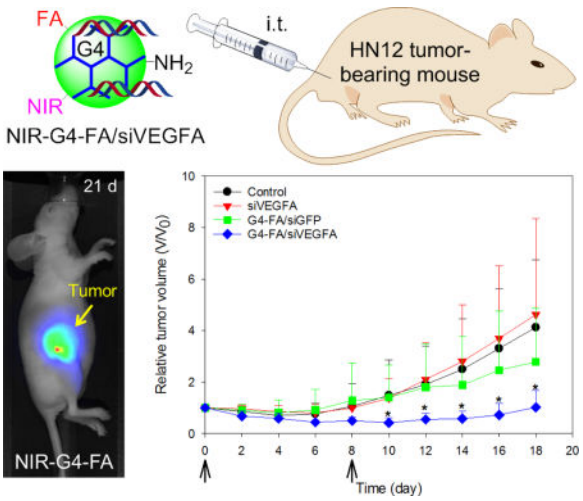

Keywords

dendrimer; targeted therapy; head and neck cancer; RNA interference; noninvasive imaging

Introduction

Head and neck squamous cell carcinomas (HNSCC) are the most common malignancy of this region [1, 2]. They arise in the mucosal epithelium of the oral cavity, pharynx, larynx and paranasal sinuses. Treatment of HNSCC often requires multimodal intervention including chemotherapy [3]. To date, small-molecular-weight anticancer drugs, such as cisplatin, docetaxel, fluorouracil, and methotrexate, remain dominant on the pharmaceutical market for treating HNSCC. These anticancer drugs interfere with DNA replication and cell division and consequently lead to cellular demise. New anticancer drugs have also been developed to target cell signaling intermediates that contribute to cancer growth. Nonetheless, incomplete tumor response and development of acquired drug resistance are common problems and may lead to systemic toxicity and disease relapse [4].

A paradigm shift in development of anticancer therapeutics has been brought about by the groundbreaking discovery of RNA interference (RNAi)[5]. RNAi has shown promise in treating cancers as it can selectively downregulate molecular targets that are responsible for proliferation, motility and survival of cancer cells or tumor stroma. Furthermore, RNAi-based cancer therapy may help reduce multidrug resistance. Molecular targets have been identified for treatment of various cancer types including HNSCC [6–8]. However, success of siRNA cancer therapy is contingent on the efficiency of the delivery system as well as the way it is administered [5, 9]. We recently tested folic acid (FA)-decorated polyamidoamine (PAMAM) dendrimer generation 4 (G4-FA) for gene delivery to HN12 head and neck cancer cells. Mechanistically, we found that G4-FA could be preferentially taken up by HN12 cells,

in which folate receptor α (FRα) is highly expressed, compared to low FRα-expressing U87 cells. In addition, G4-FA competes with free FA for the FRα on the surface of HN12 cells and facilitates FR-dependent cellular uptake of complexed plasmid DNA [10].

The fundamental understanding of G4-FA as a vector and its encouraging in vitro transfection results prompted us to test its ability to deliver siRNA to treat HNSCC in vivo in this work. It has been demonstrated that local administration of chemotherapeutics, i.e., intratumoral (i.t.) administration and convection-enhanced delivery (CED), has been found to be more efficacious than conventional systemic chemotherapy [11]. Delivery systems, including polymeric nanoparticles [12], liposomes [13], hydrogels [14], or any combinations [15, 16], have been successfully applied for localized drug delivery. Because HNSCC is localized to the oropharyngeal region, we therefore chose i.t. injection for administration of targeted therapy as it would allow substantial accumulation of nanoparticles at the tumor site and reduce toxicity to the normal tissues. Our recent work showed that G4-FA facilitated the entry of plasmid DNA into HN12 cells via FRα-mediated endocytosis at a rate much lower than that of non-specific absorptive endocytosis of plasmid mediated by unmodified G4 [10]. We hypothesized that a controlled slow tumor-specific cellular uptake mechanism would promote greater nanoparticle uptake in the tumor and enhance therapeutic effectiveness. Vascular endothelial growth factor A (VEGFA) is a major regulator of angiogenesis and promotes tumor development through its effects on the tumor microenvironment [9]. VEGFA knockdown has been shown to be effective in inhibiting tumor growth in different types of cancer. Therefore, siRNA against VEGFA (siVEGFA) was chosen as a model therapeutic siRNA in this work. Near-infrared fluorescent dye (NIR) was conjugated onto G4-FA to examine its uptake and retention in these solid tumors. We observed preferential uptake and sustained retention of NIR-G4-FA conjugates by the tumor as well as improved outcomes of G4-FA mediated localized delivery of siVEGFA in an HN12 xenograft tumor model. The study suggests that localized targeted therapy for head and neck cancer is a promising approach to promote tumor-specific uptake of siRNAs and to mitigate siRNA off-target effects.

Materials and Methods

Materials

Diaminobutane (DAB) core dendrimer generation 4.0 (technical grade) was purchased from NanoSynthons (Mt. Pleasant, MI). Dimethyl sulfoxide (DMSO), folic acid (FA), formaldehyde solution (37 wt. % in H_2O), and 1-ethyl-3-[3-dimethylaminopropyl] carbodiimide hydrochloride (EDC) were purchased from Sigma-Aldrich (St. Louis, MO). Phosphate-buffered saline (PBS) and permount mounting medium were purchased from Fisher Scientific (Pittsburgh, PA). Dulbecco's modified Eagle medium (DMEM), trypsin-EDTA (0.25%), and penicillin-streptomycin (10,000 U/mL) were purchased from Life Technologies (Carlsbad, CA). Ingenio electroporation solution was purchased from Mirus Bio (Madison, WI). Vectastain ABC kit, 3,3′-Diaminobenzidine (DAB), and hematoxylin were purchased from Vector Laboratories (Burlingame, CA). Cosmic calf serum (CS) was purchased from Lonza (Walkersville, MD). β-actin (ACTBD11B7) antibody was purchased from Santa Cruz Biotechnology (Santa Cruz, CA). VEGFA (ab46154) and CD31 (ab28364)

antibodies were purchased from Abcam (Cambridge, MA). Goat anti-rabbit antibody conjugated to horseradish peroxidase and goat anti-mouse antibody conjugated to horseradish peroxidase were purchased from Bio-Rad (Hercules, CA). SnakeSkin dialysis tubing with 7,000 molecular weight cut-off (MWCO), human VEGFA ELISA kit, ABsolute blue qPCR SYBR green low ROX mix, and Richard-Allan Scientific™ signature series Clear-Rite 3 were purchased from Thermo Scientific (Rockford, IL). IRDye 800CW NHS ester (simply referred to as NIR) was purchased from Li-COR Biotechnology (Lincoln, NE). BD Retrievagen antigen retrieval system was purchased from BD Biosciences (San Jose, CA).

Preparation of G4-FA and dendrimer/siRNA polyplexes

Details on the synthesis and characterization of G4-FA were described in our recent publication [10]. To facilitate assessment of in vivo distribution, G4 dendrimer and G4-FA conjugates were labeled with NIR dye as illustrated in Scheme 1. The custom designed siRNA against VEGFA (siVEGFA) and GFP (siGFP) were synthesized by Sigma-Aldrich (St. Louis, MO). The sequences of siRNAs are summarized in Table S1. In the initial characterization studies, dendrimer/siRNA polyplexes at various weight ratios (1/1, 5/1, and 20/1) were prepared. However, the weight ratio of 5/1 for G4-FA-based complexes was found to be optimal based on our previous work [10] and used for bioactivity evaluation in this work. G4/siRNA polyplexes (5/1, w/w) were also prepared and included as control. Briefly, 10 μg of G4-FA or G4 was diluted in 300 μL of DMEM; while 2 μg of siRNA (siVEGFA or siGFP) was diluted in 200 μL of DMEM. All the solutions were mixed by vortexing for 10 s and then equilibrated for 10 min at room temperature. The G4-FA or G4 dendrimer solution (300 μL) was mixed with the siRNA solution (200 μL), homogenized for 10 s by vortexing, and equilibrated for 30 min at room temperature. Subsequently, the volume was adjusted to 3 mL with addition of 2.5 mL of the complete medium containing 10% serum. The freshly prepared polyplexes were used immediately.

Cell culture

HN12 and HN12-YFP cells were cultured in DMEM supplemented with 10% CS, 100 units/mL of penicillin, and 100 μg/mL of streptomycin at 37 °C in 90% air/10% CO_2 [17].

Transfection

HN12 cells were seeded in the 6-well plates at a density of 20,000 cells/well and allowed to attach overnight. The cells were washed with PBS and incubated with 3 mL of polyplex-containing medium at 37 °C for 48 h. At the end of transfection, the medium was replaced with fresh complete medium containing 10% serum, and the cells were maintained under normal growth conditions for an additional 48 h. The cells treated with PBS (control) alone in the same conditions were used as negative controls. At the end of experiments, the media were collected and subjected to enzyme-linked immunosorbent assay (ELISA) for quantification of VEGFA; the cells were harvested for RNA analysis.

ELISA

The levels of VEGFA protein secreted by HN12 cells in the media were determined by a VEGFA ELISA kit. Briefly, the conditioned media were collected, and VEGFA protein concentrations were measured by ELISA as previously described [18]. An anti-human VEGFA antibody was pre-coated on the 96-well microplate. The conditioned media/standards (50 μL) were added to the antibody-coated wells and incubated for 2 h. Unbound antigen was washed away, followed by the addition of biotinylated secondary antibody and subsequent incubation for 1 h. Excess secondary antibody was washed off, and streptavidin-HRP added, which reacts with TMB (3,3′,5,5′-tetramethylbenzidine) substrate to produce a colorimetric signal. This signal was detected by measuring the absorbance at 450 nm using an Epoch plate spectrophotometer (BioTek, Winooski, VT). The number of cells in each well was measured using a Nexcelom Bioscience Cellometer Auto T4 (Nexcelom Bioscience, Lawrence, MA). Then, the VEGFA protein concentrations were normalized to the number of cells per well.

Quantitative real-time PCR (qPCR)

Relative VEGFA mRNA levels were measured by quantitative polymerase chain reaction (qPCR) as previously described [19]. Briefly, total RNA was isolated from the cells using an ISOLATE II RNA Mini Kit (Bioline, London, UK) with DNase treatment. The total RNA concentration from each sample was measured using a UV-Vis spectrophotometer (NanoDrop ND1000, Thermo Scientific, Wilmington, DE). Two μg of total RNA was used in the first-strand cDNA synthesis. qPCR was performed using SYBR green as a probe in an ABI 7500 Fast Real-Time PCR System (Applied Biosystems, Foster City, CA). Amplification of β-actin (ACTB) was used as internal control. Relative mRNA expression was quantified with the comparative cycle threshold (Ct) method and expressed as $2^{-\Delta\Delta Ct}$. The sequences of the primers are listed in Table S2.

Animal studies

All animal studies were approved by the Institutional Animal Care and Use Committee of Virginia Commonwealth University. HN12 cells or HN12-YFP cells (5×10^6 cells) were injected subcutaneously (s.c.) into the right flank of 4-week-old female athymic nude mice (Harlan Sprague Dawley, Indianapolis, IN). When the tumors had developed to a volume of 80 mm^3 (V_0) on average (8–10 days), the mice were divided into groups in a way to minimize body weight and tumor size differences among the groups before they received treatments as indicated in Table S3. Time-dependent whole-body fluorescence images were recorded using a Pearl Trilogy small animal imaging system (Li-COR Biotechnology, Lincoln, NE). Body weights were recorded, and tumors were measured by standard digital caliper (Tresna, Guangxi Province, China) every other day. Tumor volume was determined by using the formula $V = Length\times Width^2/2$, with the width being smaller than the length [20]. Relative tumor volume (V/V_0) was reported. In the HN12-YFP tumor-bearing mice, the mice were imaged using an IVIS 200 system to monitor tumor size. The mice were euthanized at the end of experiment or when signs of discomfort were detected by the investigator or as recommended by the veterinarian who monitored the mice daily to investigate animal survival. A tumor volume of 320 mm^3 was used as a threshold value to

report animal survival rate following the same strategy as described previously [21]. Organs including heart, kidney, spleen, lung, liver, brain, and tumor were collected and imaged. Odyssey CLx infrared imaging system software (Li-COR Biotechnology, Lincoln, NE) was used for image analysis. Dye accumulation in the organs was evaluated by calculating the contrast index values [22]. The collected tumors were then fixed in 10% neutral-buffered formalin for histologic evaluation.

Hematoxylin and eosin (H&E) staining

Formalin-fixed tumor specimens were embedded in paraffin and sectioned at 5 μm. H&E staining was performed at the VCU Massey Cancer Biological Macromolecule Core Facility. The tissue slides were imaged under a Nikon ECLIPSE E400 clinical microscope (Nikon Instruments Inc., Melville, NY) using a magnificat ion of 200×.

Immunohistochemical (IHC) staining

IHC staining was carried out following procedures described previously [23]. Briefly, the paraffin-embedded tumor sections were deparaffinized in Clear-Rite 3 and rehydrated in graded alcohols (100, 95, 90, 80, and 70%). For antigen retrieval, the sections were microwaved in BD Retrievagen buffer for 10 min. Endogenous peroxidase activity was quenched by incubation in 3% (v/v) H_2O_2 for 15 min. The sections were incubated with anti-CD31 antibody at 1:100 dilution for 1 h. Subsequently, the sections were washed with TBS, and the immobilized antibodies were detected using the ABC kit. DAB and hematoxylin were used as the chromogen and the nuclear counterstain, respectively. The primary antibody was omitted as a negative control. The tissues slides were then imaged under a Nikon ECLIPSE E400 clinical microscope using a magnification of 200×. The average microvessel counts (per 200× field) were quantitated as the number of CD31-positive vessels in six randomly selected fields for each sample, and each group included sections from 2 mice.

Statistical analysis

The data are expressed as means ± standard deviation (SD). The data were analyzed using one-way analysis of variance (ANOVA) followed by Holm-Sidak method for subgroup comparison or using t-test for two-group comparison with the control. A value of $p < 0.05$ was considered statistically significant.

Results

Characterization of dendrimers and their polyplexes

The zeta potential of G4 or FA-functionalized (or NIR-labeled) G4 and their polyplexes is summarized in Table S4. G4 and G4 derivatives exhibited high positive zeta potentials although a decrease in zeta potential was observed as a result of various degrees of surface modification. G4-FA can complex with siVEGFA at various weight ratios. At a weight ratio of 1/1, the polyplexes show a negative zeta potential, most likely due to less G4-FA molecules than siVEGFA molecules (molar ratio of 0.8/1). In contrast, at the weight ratios of 5/1 and 20/1, the polyplexes showed positive zeta potentials as G4-FA outnumbered siVEGFA (molar ratio of 4.2/1 and 16.9/1, respectively). We chose the weight ratio of 5/1 to

form G4-FA/siRNA polyplexes for the rest of the work for the following reasons: G4-FA displayed the highest efficiency of gene transfection in HN12 cells seen in our previous work [10]; and the less positive zeta potential can reduce non-specific cellular uptake of polyplexes [24]. For comparison, G4/siRNA polyplexes were prepared at the same weight ratio and tested along with G4-FA/siRNA polyplexes.

Enhanced VEGFA knockdown in vitro by G4-FA

We first validated that only siVEGFA but not siGFP was able to reduce VEGFA mRNA and protein expression levels using electroporation (Figure S1A,B). Furthermore, siGFP complexed with G4-FA did not show any knockdown effects on VEGFA either (Figure S1C,D). Therefore, G4-FA/siGFP was used as a nontherapeutic control in this work. Both G4 and G4-FA were shown to be able to deliver siVEGFA efficiently and resulted in significant knockdown of VEGFA in mRNA expression and protein secretion in vitro ($p<0.001$). Further analysis revealed that G4-FA/siVEGFA showed higher knockdown efficiency. The reduction of VEGFA mRNA expression and protein release by G4-FA/siVEGFA was stronger compared to the reduction by G4/siVEGFA ($p<0.001$ and $p<0.01$, respectively) (Figure 1A,B), consistent with our previous findings [10].

G4-FA exhibits high tumor uptake and sustained retention

One of the key advantages of targeted dendrimers for anti-cancer drug delivery is that these dendrimers can facilitate nanoparticle and drug accumulation within tumors. We conjugated NIR onto the dendrimers (NIR-G4 and NIR-G4-FA) to enable real-time in vivo tracking of the dendrimer vectors following i.t. administration. For comparison, free NIR was also included in the study.

Following i.t. administration of a single dose of NIR, NIR-G4 and NIR-G4-FA, NIR fluorescence whole-body images of mice were taken over a period of 21 days (Figure 2A). To understand retention kinetics of these formulations, relative tumor fluorescence intensity kinetics profiles of the three formulations with respect to the tumor fluorescence intensity at day 0 (immediately after injection) are shown in Figure 2B. At the end, the tumor-bearing mice were sacrificed, and the major organs were collected for quantitative analysis. Not surprisingly, free NIR had limited retention in the tumor. The fluorescence signal detected in the tumor at 1 h significantly decreased after 1 day and completely vanished after 3 days ($p<0.001$) (Figure 2B). The ventral view of the mice at 1 h-post i.t. injection of free NIR showed a significant fluorescence signal in the bladder in addition to the whole body (Figure S2), suggesting NIR was being eliminated from the body via renal clearance as a result of poor retention by the tumor. Both NIR-G4 and NIR-G4-FA groups showed strong and stable fluorescence signal in the tumor region up to 21 d. The ventral view of the mice at 1 h shows the fluorescence signal was highly localized in the tumor region (Figure S2). These observations indicated both NIR-G4 and NIR-G4-FA had high uptake and sustained retention in the tumor or its surrounding tissue. As shown in Figure 2B, an initial dip in the fluorescence intensity was observed in NIR-G4 during the first week ($p<0.01$ for days 1, 3 vs day 0, $p<0.05$ for day 7 vs. day 0), likely because of skin lesions or leakage/clearance of NIR-G4 out of the tumor (Figure S4). The increased fluorescence intensities afterwards might be due to the direct or close exposure of NIR dyes to the detector when the tumor

grew rapidly. In contrast, NIR-G4-FA exhibited invariably high tumor retention within the observation window. There were no significant body weight differences among the mice in the three groups (Figure 2C).

Major organs and tumor tissues were excised at the end of experiment and subjected to fluorescence imaging (Figure 2D). The NIR fluorescence signal of NIR-G4 and NIR-G4-FA was mostly observed within the tumors but was barely seen in the other organs. Consistent with in vivo imaging, no noticeable accumulation of free dye was observed in the tumors. Quantitative analysis of fluorescence intensities normalized to tumor mass reveals the complete clearance of free NIR (Figure 2E). The mean tumor fluorescence intensity (counts/mg) in the NIR-G4-FA group was nearly twice as strong as that in the NIR-G4 group, suggesting high tumor uptake and long retention of NIR-G4-FA as a drug and gene carrier.

Single-dose antitumor effects

VEGFs play central roles in regulation of angiogenesis. VEGFA, a major angiogenic factor, regulates endothelial cell proliferation, migration, vascular permeability, secretion, and other endothelial cell functions [25]. The VEGF-VEGFR interaction is crucial not only for physiological angiogenesis from early embryonic to adult stages but also for pathological angiogenesis, such as in cancer [25]. To date, strategies have been developed to target the VEGF-VEGFR system for anti-angiogenic therapy alone or in combination with other modalities for cancer treatment [26–29]. In this study, we evaluated the antitumor effects of i.t. administered G4-FA/siVEGFA in HN12 tumor-bearing nude mice. G4-FA/siGFP and PBS-treated mice were included as control groups.

Following i.t. administration of a single-dose of G4-FA/siVEGFA, G4-FA/siGFP, and PBS, tumor volume and body weight of the treated mice were measured every other day. As shown in Figure 3A, G4-FA/siGFP did not show antitumor effects as the G4-FA/siGFP and PBS groups showed tumor growth curves similar to one another. In contrast, significantly reduced tumor volumes ($p<0.05$) in the G4-FA/siVEGFA group were observed at day 16 and day 18. The body weights of the mice treated with G4-FA/siVEGFA and G4-FA/siGFP were similar to those of the control treated with PBS (Figure 3B). Although one dose of G4-FA/siVEGFA had an effect, tumor volume started increasing at day 8. This led us to develop a two-dose regimen with a second dose injection at day 8 to examine whether tumor growth can be further inhibited.

Two-dose antitumor effects

The single-dose experiment showed antitumor activity of G4-FA/siVEGFA. To test whether or not tumor growth could be further retarded, we conducted a two-dose regimen experiment, in which one dose was given at day 0 and a second dose was inoculated at day 8. In this experiment, we used YFP-expressing HN12 cells to establish a xenograft tumor model that allowed for real-time fluorescence imaging of tumors, complementary to direct tumor volume measurement. We then monitored tumor growth in the mice receiving two doses of PBS, siVEGFA, G4-FA/siGFP, G4/siVEGFA, and G4-FA/siVEGFA (8 days apart between the two doses) via i.t. administration. Due to severe skin lesion observed in the G4/

siVEGFA group, this group was sacrificed early and excluded from further analysis and comparison (Figure S4). This was the only group that experienced body weight loss after the second dose (data not shown).

Similar to the single dose modality, a second dose of siVEGFA and G4-FA/siGFP did not show inhibitory effects on tumor growth (Figure 4A). Strikingly, a second dose of G4-FA/siVEGFA brought about a nearly complete inhibition in increase of tumor volume during the observation window. Tumor volume differences between the G4-FA/siVEGFA group and the control groups became significant beginning at day 10 ($p<0.05$). Using a threshold of tumor volume 320 mm^3 to assess animal survival, the G4-FA/siVEGFA had a 100% survival rate (Figure 4B). No body weight differences were noticed (Figure 4C). H&E staining of tumor tissues did not reveal any histological differences among the tested groups (Figure 4D). This confirmed good tissue compatibility of G4-FA/siVEGFA. siVEGFA delivered by G4-FA was expected to reduce angiogenesis within the tumor. CD31 is an endothelial cell surface marker, which is routinely used to demonstrate the presence of endothelial cells in histological tissue sections [29, 30]. The IHC staining of CD31 illustrated an obvious decrease in CD31-positive tumor microvessels of the G4-FA/siVEGFA group, which was supported by the quantitative vessel counts (Figure 4E). The average vessel counts (per 200× field) in the control, siVEGFA, and G4-FA/siGFP groups were in the range of 15.0–16.3, similar to the value reported in the literature [31]. In contrast, G4-FA/siVEGFA reduced the microvessel count to 6.8, representing a 58% decrease as compared to the control group.

During the two-dose experiment, we employed an IVIS 200 system for noninvasive imaging of YFP-expressing tumors and semi-quantitative assessment of antitumor activity of the formulations (Figure 5A). YFP fluorescence intensity increase was correlated to tumor growth. The mean YFP fluorescence intensity of the G4-FA/siVEGFA at Day 16 was the lowest ($p<0.05$), thus reflecting their smallest tumor volume (Figure 5B). The tumor reduction trend assessed by noninvasive imaging was consistent with direct tumor volume measurements.

Discussion

Compared to systemic administration of chemotherapeutics, localized drug delivery holds several distinct advantages including reduced systemic toxicity, sustained local drug release, increased drug bioavailability, collectively promoting chemotherapy efficacy [32]. Our study strongly suggests G4-FA is able to deliver siVEGFA to the tumor through localized delivery, reducing tumor angiogenesis and inhibiting growth of head and neck tumors.

NIR dyes have attracted considerable attention as diagnostic agents in the field of cancer research as a result of their high tissue penetration depth, low tissue autofluorescence interference in the NIR spectrum window, and improved tumor-to-background ratio value [33]. Glionlan, 5-Aminolevulinic acid-induced protoporphyrin IX, has been used clinically for distinguishing malignant glioma from normal brain tissue [34]. Bevacizumab, IRDye800CW conjugated with antibody against VEGFA, is currently undergoing clinical trials for early cancer detection [35]. NIR dyes have been incorporated via various strategies, including NIR dye-ligand conjugates [36, 37], activatable NIR dyes [38], and NIR dye-

encapsulated or - conjugated nanoparticles [39–41] for tumor diagnosis. In this work, we utilized NIR dye as an imaging agent and investigated the biodistribution of NIR-G4-FA. Our results demonstrate that NIR-G4-FA has high tumor uptake and extended retention in the tumor. This finding agrees well with our in vitro results that G4-FA is preferentially taken up by FRα highly-expressing HN12 cells and internalized via FRα-mediated endocytosis [10]. Localized delivery of G4-FA would be expected to promote preferential nanoparticle accumulation in the tumor while avoiding high uptake by the kidney, spleen, and liver resulting from introduction through the systemic circulation. We found that G4-FA enables prolonged siRNA (i.e., siVEGFA) delivery and sustained knockdown effect locally, as judged by the reduced tumor vascularization, and subsequently suppressed tumor growth.

Additionally, we studied the biodistribution of NIR-G4-FA following i.v. administration. We found that NIR-G4-FA did not specifically accumulate in the tumor via systemic delivery. G4-FA clearance may involve both hepatic and renal clearance pathways as these nanoparticles primarily accumulated in the kidney, liver, and spleen (Figure S3). G4-FA was rapidly taken up by the kidney, spleen, and liver, in large part due to the high folic acid intake activities in these organs [42–44]. Poor accumulation of G4-FA in the tumor via the i.v. route is most likely due to its short circulation half-life and/or insufficient EPR effect. Thus, if G4-FA were to be used for systemic gene delivery, a PEGylated delivery system would be helpful as PEG can significantly prolong the circulation half-life of nanoparticles [45–48]. In this scenario, FA would be preferably conjugated to the terminal end of a PEG spacer to prevent the shielding effect on the targeting ability of the delivery system. Incorporation of a protonable linkage for dendrimer PEGylation may help improve the buffering capacity of the dendrimer vector for enhanced gene transfection [49].

Overcoming experimental limitations observed in our studies can further enhance therapeutic outcomes. We noticed that the silencing potency of a single set of siVEGFA duplexes was modest in HN12 cells (Figure S1). In addition, the transfection was carried out in the presence of serum, raising the possibility that the serum proteins may interact with dendrimer/siRNA polyplexes to destabilize them [50]. Therefore, complexing G4-FA with a pool of siVEGFA duplex sets may help improve the knockdown efficiency. Increased understanding of molecular events involved in HNSCC initiation and progression has led to the identification of a number of genes as potential therapeutics for HNSCC gene therapy, including Hsp65 gene and eIF-4E, STAT3, POU2F1, and EPS8 siRNA/shRNA [5, 51–54]. Combining potent siRNA(s) with the FR-targeted dendrimer vector will likely yield better effects in treating HNSCC. Our in vitro and in vivo studies demonstrate that G4-FA is a relatively safe FRα-targeted gene delivery vehicle although repeated dosing is necessary to exert a sustained tumor suppressing effect. Long-term toxicity and nanoparticle clearance following repeated dosing will be assessed in future work.

Conclusions

Our work has demonstrated that folic acid-decorated PAMAM dendrimer shows high tumor uptake and sustained retention following intratumoral injection. The local delivery of FR-targeted PAMAM dendrimer G4 complexed with siVEGFA resulted in pronounced tumor suppression in an HN12 xenograft tumor model. Tumor suppression was attributed to

enhanced tumor uptake of siRNA and prolonged nanoparticle retention in the tumor. Repeated doses of G4-FA/siVEGFA would be necessary to lead to strong and sustained tumor inhibition effects. Taken together, G4-FA is a tumor-specific safe siRNA delivery system that provides a platform to promote tumor-specific uptake of siRNAs and to mitigate siRNA off-target effects for localized targeted therapy for head and neck cancer.

Supplementary Material

Refer to Web version on PubMed Central for supplementary material.

Acknowledgments

This work was supported, in part, by the National Science Foundation (CAREER award CBET0954957), and the National Institutes of Health (R01EY024072 and R01DE024381).

References

1. Brunotto M, Zarate AM, Bono A, Barra JL, Berra S. Risk genes in head and neck cancer: A systematic review and meta-analysis of last 5years. Oral Oncol. 2014; 50(3):178–188. [PubMed: 24370206]
2. Du Y, Peyser ND, Grandis JR. Integration of molecular targeted therapy with radiation in head and neck cancer. Pharmacology & Therapeutics. 2014; 142(1):88–98. [PubMed: 24280066]
3. Klein J, Livergant J, Ringash J. Health related quality of life in head and neck cancer treated with radiation therapy with or without chemotherapy: A systematic review. Oral Oncology. 2014; 50(4): 254–262. [PubMed: 24559650]
4. Dobbelstein M, Moll U. Targeting tumour-supportive cellular machineries in anticancer drug development. Nat Rev Drug Discov. 2014; 13(3):179–96. [PubMed: 24577400]
5. Xu L, Yeudall WA, Yang H. Dendrimer-Based RNA Interference Delivery for Cancer Therapy, Tailored Polymer Architectures for Pharmaceutical and Biomedical Applications. American Chemical Society. 2013:197–213.
6. Han JB, Tao ZZ, Chen SM, Kong YG, Xiao BK. Adenovirus-mediated transfer of tris-shRNAs induced apoptosis of nasopharyngeal carcinoma cell in vitro and in vivo. Cancer Lett. 2011; 309(2): 162–9. [PubMed: 21669490]
7. Lo WL, Chien Y, Chiou GY, Tseng LM, Hsu HS, Chang YL, Lu KH, Chien CS, Wang ML, Chen YW, Huang PI, Hu FW, Yu CC, Chu PY, Chiou SH. Nuclear localization signal-enhanced RNA interference of EZH2 and Oct4 in the eradication of head and neck squamous cell carcinoma-derived cancer stem cells. Biomaterials. 2012; 33(14):3693–709. [PubMed: 22361100]
8. Rahman MA, Amin AR, Wang X, Zuckerman JE, Choi CH, Zhou B, Wang D, Nannapaneni S, Koenig L, Chen Z, Chen ZG, Yen Y, Davis ME, Shin DM. Systemic delivery of siRNA nanoparticles targeting RRM2 suppresses head and neck tumor growth. Journal of controlled release: official journal of the Controlled Release Society. 2012; 159(3):384–92. [PubMed: 22342644]
9. Brenner MK, Gottschalk S, Leen AM, Vera JF. Is cancer gene therapy an empty suit? Lancet Oncol. 2013; 14(11):e447–56. [PubMed: 24079872]
10. Xu L, Kittrell S, Yeudall WA, Yang H. Folic acid-decorated polyamidoamine dendrimer mediates selective uptake and high expression of genes in head and neck cancer cells. Nanomedicine (Lond). 2016; 11(22):2959–2973. [PubMed: 27781559]
11. Fakhari A, Subramony JA. Engineered in-situ depot-forming hydrogels for intratumoral drug delivery. Journal of controlled release: official journal of the Controlled Release Society. 2015; 220(Pt A):465–75. [PubMed: 26585504]
12. You J, Zhao J, Wen X, Wu C, Huang Q, Guan F, Wu R, Liang D, Li C. Chemoradiation therapy using cyclopamine-loaded liquid-lipid nanoparticles and lutetium-177-labeled core-crosslinked

polymeric micelles. Journal of controlled release: official journal of the Controlled Release Society. 2015; 202:40–8. [PubMed: 25637565]

13. Peddada LY, Garbuzenko OB, Devore DI, Minko T, Roth CM. Delivery of antisense oligonucleotides using poly(alkylene oxide)-poly(propylacrylic acid) graft copolymers in conjunction with cationic liposomes. Journal of controlled release: official journal of the Controlled Release Society. 2014; 194:103–12. [PubMed: 25192941]
14. Price R, Poursaid A, Cappello J, Ghandehari H. In vivo evaluation of matrix metalloproteinase responsive silk-elastinlike protein polymers for cancer gene therapy. Journal of controlled release: official journal of the Controlled Release Society. 2015; 213:96–102. [PubMed: 26095079]
15. Xu HL, Mao KL, Lu CT, Fan ZL, Yang JJ, Xu J, Chen PP, ZhuGe DL, Shen BX, Jin BH, Xiao J, Zhao YZ. An injectable acellular matrix scaffold with absorbable permeable nanoparticles improves the therapeutic effects of docetaxel on glioblastoma. Biomaterials. 2016; 107:44–60. [PubMed: 27614158]
16. Lalloo A, Chao P, Hu P, Stein S, Sinko PJ. Pharmacokinetic and pharmacodynamic evaluation of a novel in situ forming poly(ethylene glycol)-based hydrogel for the controlled delivery of the camptothecins. Journal of controlled release: official journal of the Controlled Release Society. 2006; 112(3):333–42. [PubMed: 16650910]
17. Yuan Q, Lee E, Yeudall WA, Yang H. Dendrimer-triglycine-EGF nanoparticles for tumor imaging and targeted nucleic acid and drug delivery. Oral Oncol. 2010; 46(9):698–704. [PubMed: 20729136]
18. Xu L, Sheybani N, Ren S, Bowlin GL, Yeudall WA, Yang H. Semi-Interpenetrating Network (sIPN) Co-Electrospun Gelatin/Insulin Fiber Formulation for Transbuccal Insulin Delivery. Pharm Res. 2015; 32(1):275–85. [PubMed: 25030186]
19. Xu L, Bai Q, Rodriguez-Agudo D, Hylemon PB, Heuman DM, Pandak WM, Ren S. Regulation of hepatocyte lipid metabolism and inflammatory response by 25-hydroxycholesterol and 25-hydroxycholesterol-3-sulfate. Lipids. 2010; 45(9):821–32. [PubMed: 20700770]
20. Guo S, Lin CM, Xu Z, Miao L, Wang Y, Huang L. Co-delivery of cisplatin and rapamycin for enhanced anticancer therapy through synergistic effects and microenvironment modulation. ACS Nano. 2014; 8(5):4996–5009. [PubMed: 24720540]
21. Caruana I, Savoldo B, Hoyos V, Weber G, Liu H, Kim ES, Ittmann MM, Marchetti D, Dotti G. Heparanase promotes tumor infiltration and antitumor activity of CAR-redirected T lymphocytes. Nat Med. 2015; 21(5):524–9. [PubMed: 25849134]
22. Yue C, Liu P, Zheng M, Zhao P, Wang Y, Ma Y, Cai L. IR-780 dye loaded tumor targeting theranostic nanoparticles for NIR imaging and photothermal therapy. Biomaterials. 2013; 34(28): 6853–61. [PubMed: 23777910]
23. Zhang X, Bai Q, Xu L, Kakiyama G, Pandak WM Jr, Zhang Z, Ren S. Cytosolic sulfotransferase 2B1b promotes hepatocyte proliferation gene expression in vivo and in vitro. Am J Physiol Gastrointest Liver Physiol. 2012; 303(3):G344–55. [PubMed: 22679001]
24. Ingle NP, Malone B, Reineke TM. Poly(glycoamidoamine)s: a broad class of carbohydrate-containing polycations for nucleic acid delivery. Trends Biotechnol. 2011; 29(9):443–53. [PubMed: 21705101]
25. Shibuya M. Vascular endothelial growth factor and its receptor system: physiological functions in angiogenesis and pathological roles in various diseases. J Biochem. 2013; 153(1):13–9. [PubMed: 23172303]
26. Kim SH, Jeong JH, Kim TI, Kim SW, Bull DA. VEGF siRNA delivery system using arginine-grafted bioreducible poly(disulfide amine). Mol Pharm. 2009; 6(3):718–26. [PubMed: 19055368]
27. Kim WJ, Christensen LV, Jo S, Yockman JW, Jeong JH, Kim YH, Kim SW. Cholesteryl oligoarginine delivering vascular endothelial growth factor siRNA effectively inhibits tumor growth in colon adenocarcinoma. Mol Ther. 2006; 14(3):343–50. [PubMed: 16765648]
28. Takei Y, Nemoto T, Mu P, Fujishima T, Ishimoto T, Hayakawa Y, Yuzawa Y, Matsuo S, Muramatsu T, Kadomatsu K. In vivo silencing of a molecular target by short interfering RNA electroporation: tumor vascularization correlates to delivery efficiency. Mol Cancer Ther. 2008; 7(1):211–21. [PubMed: 18202023]

29. Thaci B, Ulasov IV, Ahmed AU, Ferguson SD, Han Y, Lesniak MS. Anti-angiogenic therapy increases intratumoral adenovirus distribution by inducing collagen degradation. Gene Ther. 2013; 20(3):318–27. [PubMed: 22673390]
30. Wang H, Patel V, Miyazaki H, Gutkind JS, Yeudall WA. Role for EPS8 in squamous carcinogenesis. Carcinogenesis. 2009; 30(1):165–74. [PubMed: 19008210]
31. Wang X, Li J, Wang Y, Koenig L, Gjyrezi A, Giannakakou P, Shin EH, Tighiouart M, Chen ZG, Nie S, Shin DM. A folate receptor-targeting nanoparticle minimizes drug resistance in a human cancer model. ACS Nano. 2011; 5(8):6184–94. [PubMed: 21728341]
32. Norouzi M, Nazari B, Miller DW. Injectable hydrogel-based drug delivery systems for local cancer therapy. Drug Discov Today. 2016
33. Yuan A, Wu J, Tang X, Zhao L, Xu F, Hu Y. Application of near-infrared dyes for tumor imaging, photothermal, and photodynamic therapies. J Pharm Sci. 2013; 102(1):6–28. [PubMed: 23132644]
34. Slof J, Diez Valle R, Galvan J. Cost-effectiveness of 5-aminolevulinic acid-induced fluorescence in malignant glioma surgery. Neurologia. 2015; 30(3):163–8. [PubMed: 24468659]
35. Chang K, Zhang B, Guo X, Zong M, Rahman R, Sanchez D, Winder N, Reardon DA, Zhao B, Wen PY, Huang RY. Multimodal imaging patterns predict survival in recurrent glioblastoma patients treated with bevacizumab. Neuro Oncol. 2016; 18(12):1680–1687. [PubMed: 27257279]
36. Hanawa M, Suzuki S, Dobashi Y, Yamane T, Kono K, Enomoto N, Ooi A. EGFR protein overexpression and gene amplification in squamous cell carcinomas of the esophagus. Int J Cancer. 2006; 118(5):1173–80. [PubMed: 16161046]
37. Jin ZH, Josserand V, Foillard S, Boturyn D, Dumy P, Favrot MC, Coll JL. In vivo optical imaging of integrin alphaV-beta3 in mice using multivalent or monovalent cRGD targeting vectors. Mol Cancer. 2007; 6:41. [PubMed: 17565663]
38. Pham W, Choi Y, Weissleder R, Tung CH. Developing a peptide-based near-infrared molecular probe for protease sensing. Bioconjug Chem. 2004; 15(6):1403–7. [PubMed: 15546208]
39. Chen Y, Li H, Deng Y, Sun H, Ke X, Ci T. Near-infrared light triggered drug delivery system for higher efficacy of combined chemo-photothermal treatment. Acta Biomater. 2017
40. Xia B, Wang B, Shi J, Zhang Y, Zhang Q, Chen Z, Li J. Photothermal and biodegradable polyaniline/porous silicon hybrid nanocomposites as drug carriers for combined chemo-photothermal therapy of cancer. Acta Biomater. 2017
41. Wu J, Zhou Y, Li S, Qu D, Zhu WH, Tian H. Real-time near-infrared bioimaging of a receptor-targeted cytotoxic dendritic theranostic agent. Biomaterials. 2017; 120:1–10. [PubMed: 28011190]
42. Chen C, Ke J, Zhou XE, Yi W, Brunzelle JS, Li J, Yong EL, Xu HE, Melcher K. Structural basis for molecular recognition of folic acid by folate receptors. Nature. 2013; 500(7463):486–9. [PubMed: 23851396]
43. Tarantino G, Scalera A, Finelli C. Liver-spleen axis: intersection between immunity, infections and metabolism. World J Gastroenterol. 2013; 19(23):3534–42. [PubMed: 23801854]
44. Xu L, Bai Q, Zhang X, Yang H. Folate-mediated chemotherapy and diagnostics: An updated review and outlook. Journal of controlled release: official journal of the Controlled Release Society. 2017; 252:73–82. [PubMed: 28235591]
45. Pasut G, Paolino D, Celia C, Mero A, Joseph AS, Wolfram J, Cosco D, Schiavon O, Shen H, Fresta M. Polyethylene glycol (PEG)-dendron phospholipids as innovative constructs for the preparation of super stealth liposomes for anticancer therapy. Journal of controlled release: official journal of the Controlled Release Society. 2015; 199:106–13. [PubMed: 25499917]
46. van Vlerken LE, Vyas TK, Amiji MM. Poly(ethylene glycol)-modified nanocarriers for tumor-targeted and intracellular delivery. Pharm Res. 2007; 24(8):1405–14. [PubMed: 17393074]
47. Xiao J, Duan X, Yin Q, Zhang Z, Yu H, Li Y. Nanodiamonds-mediated doxorubicin nuclear delivery to inhibit lung metastasis of breast cancer. Biomaterials. 2013; 34(37):9648–56. [PubMed: 24016858]
48. Zhang Y, Velasco O, Zhang X, Ting K, Soo C, Wu BM. Bioactivity and circulation time of PEGylated NELL-1 in mice and the potential for osteoporosis therapy. Biomaterials. 2014; 35(24): 6614–21. [PubMed: 24818884]

49. Yuan Q, Yeudall WA, Yang H. PEGylated polyamidoamine dendrimers with bis-aryl hydrazone linkages for enhanced gene delivery. Biomacromolecules. 2010; 11(8):1940–7. [PubMed: 20593893]

50. Liu C, Liu X, Rocchi P, Qu F, Iovanna JL, Peng L. Arginine-terminated generation 4 PAMAM dendrimer as an effective nanovector for functional siRNA delivery in vitro and in vivo. Bioconjug Chem. 2014; 25(3):521–32. [PubMed: 24494983]

51. Fan TF, Wu TF, Bu LL, Ma SR, Li YC, Mao L, Sun ZJ, Zhang WF. Dihydromyricetin promotes autophagy and apoptosis through ROS-STAT3 signaling in head and neck squamous cell carcinoma. Oncotarget. 2016

52. Amornphimoltham P, Patel V, Sodhi A, Nikitakis NG, Sauk JJ, Sausville EA, Molinolo AA, Gutkind JS. Mammalian target of rapamycin, a molecular target in squamous cell carcinomas of the head and neck. Cancer Res. 2005; 65(21):9953–61. [PubMed: 16267020]

53. Michaluart P, Abdallah KA, Lima FD, Smith R, Moyses RA, Coelho V, Victora GD, Socorro-Silva A, Volsi EC, Zarate-Blades CR, Ferraz AR, Barreto AK, Chammas MC, Gomes R, Gebrim E, Arakawa-Sugueno L, Fernandes KP, Lotufo PA, Cardoso MR, Kalil J, Silva CL. Phase I trial of DNA-hsp65 immunotherapy for advanced squamous cell carcinoma of the head and neck. Cancer Gene Ther. 2008; 15(10):676–84. [PubMed: 18535616]

54. Sharpe DJ, Orr KS, Moran M, White SJ, McQuaid S, Lappin TR, Thompson A, James JA. POU2F1 activity regulates HOXD10 and HOXD11 promoting a proliferative and invasive phenotype in head and neck cancer. Oncotarget. 2014; 5(18):8803–15. [PubMed: 25301728]

Statement of Significance

Head and neck squamous cell carcinoma (HNSCC) is the sixth most common cancer worldwide and is difficult to transfect for gene therapy. We developed folate receptor (FA)-targeted polyamidoamine (PAMAM) dendrimer for enhanced delivery of genes to HNSCC and gained in-depth understanding of how gene delivery and transfection in head and neck squamous cancer cells can be enhanced via FR-targeted PAMAM dendrimers. The results we report here are encouraging and present latest advances in using dendrimers for cancer therapies, in particular for HNSCC. Our work has demonstrated that localized delivery of FR-targeted PAMAM dendrimer G4 complexed with siVEGFA resulted in pronounced tumor suppression in an HN12 xenograft tumor model. Tumor suppression was attributed to enhanced tumor uptake of siRNA and prolonged nanoparticle retention and infiltration in the tumor. Taken together, G4-FA shows high tumor uptake and sustained highly localized retention properties, making it a suitable platform for local delivery of siRNAs to treat cancers that are readily accessible for injection of therapeutics such as HNSCC.

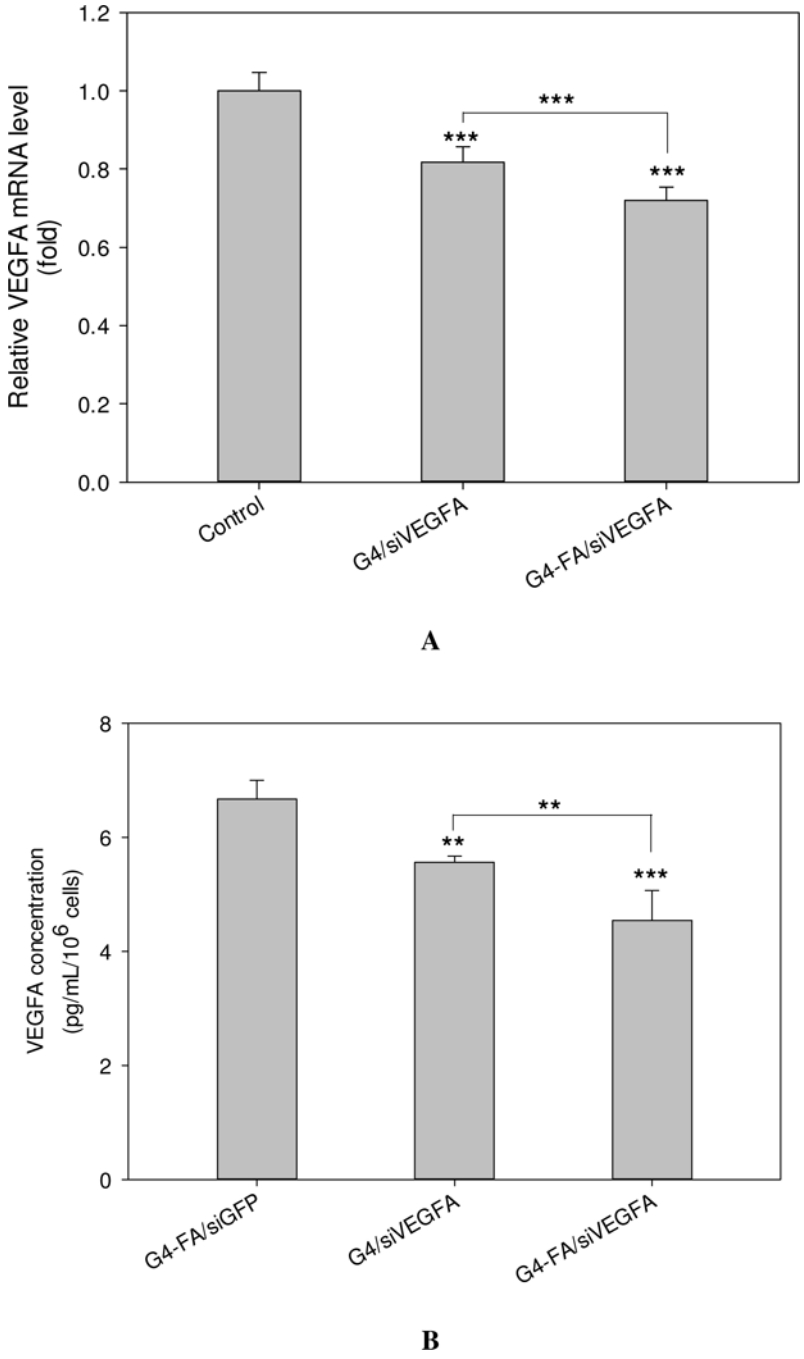

Figure 1.

In vitro assessment of VEGFA knockdown. HN12 cells were treated with PBS (control), G4-FA/siGFP, G4/siVEGFA, or G4-FA/siVEGFA (5:1, w/w) for 48 h, followed by an additional 48 h-culture. (A) The relative mRNA expression of VEGFA as determined by qPCR analysis, and normalized to β-actin. (B) The protein concentration of VEGFA released into the medium as determined by ELISA, and normalized to cell number. ** indicates $p < 0.01$ versus the control, and *** indicates $p < 0.001$ versus the control or for the indicated two-group comparison (n=5–6).

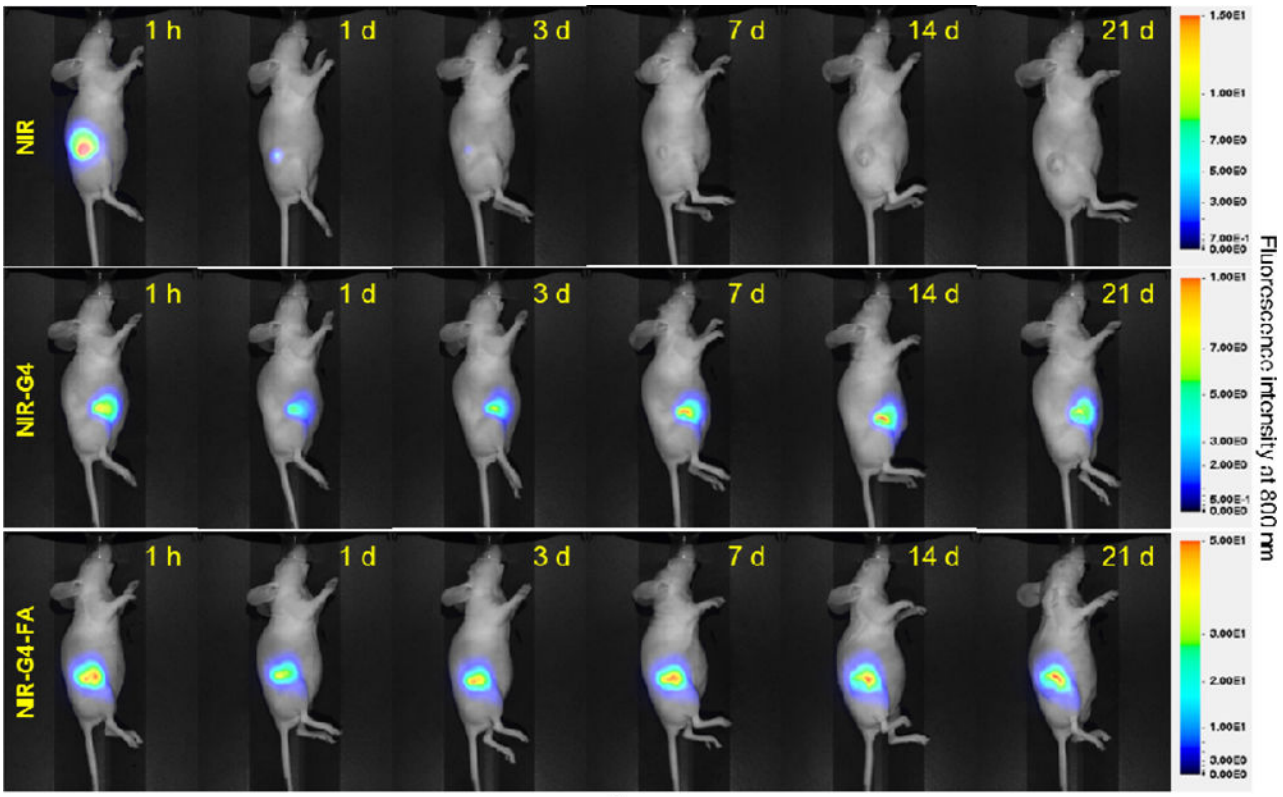

A

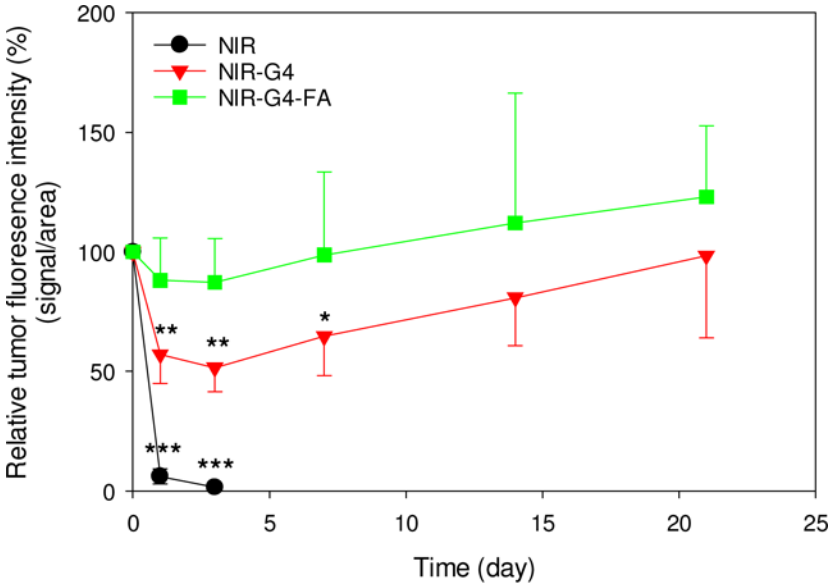

B

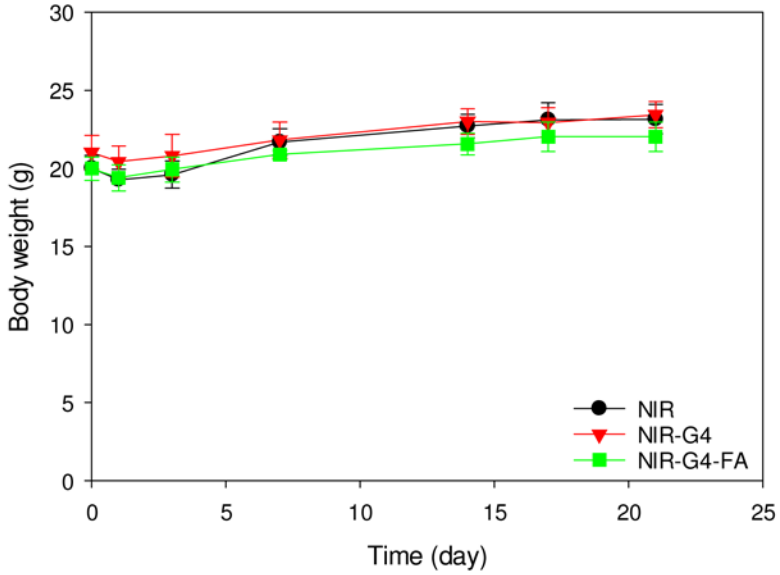

C

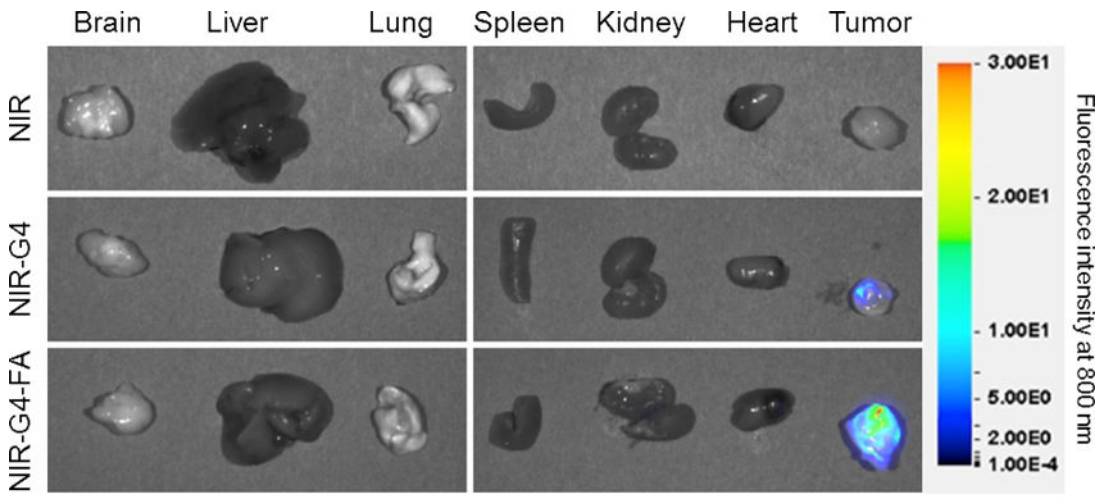

D

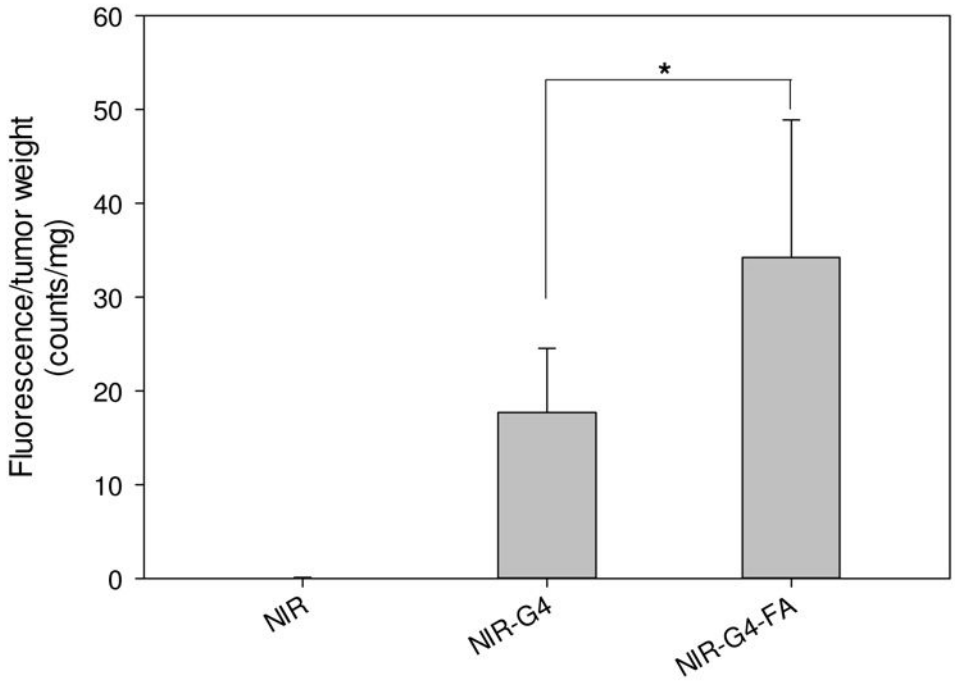

E

Figure 2.

In vivo assessment of retention and uptake of dendritic nanoparticles in tumors. Real-time imaging of HN12 tumor-bearing mice following i.t. injection of NIR, NIR-G4, or NIR-G4-FA. (A) Whole-body images of representative mice taken at the indicated time points up to 21 days. (B) Relative fluorescence intensities in the tumor region determined by normalizing to the initial fluorescence intensity of each group. * $p < 0.05$, ** $p < 0.01$, *** $p < 0.001$ versus initial time point in each group (n = 5). (C) Body weights of mice in all groups monitored during the experiment. (D) Fluorescence images of representative major organs

taken immediately after the mice were sacrificed at day 21. (E) Quantitative fluorescence intensities at the tumor site (signal counts per tumor weight). * $p < 0.05$ for the indicated two-group comparison.

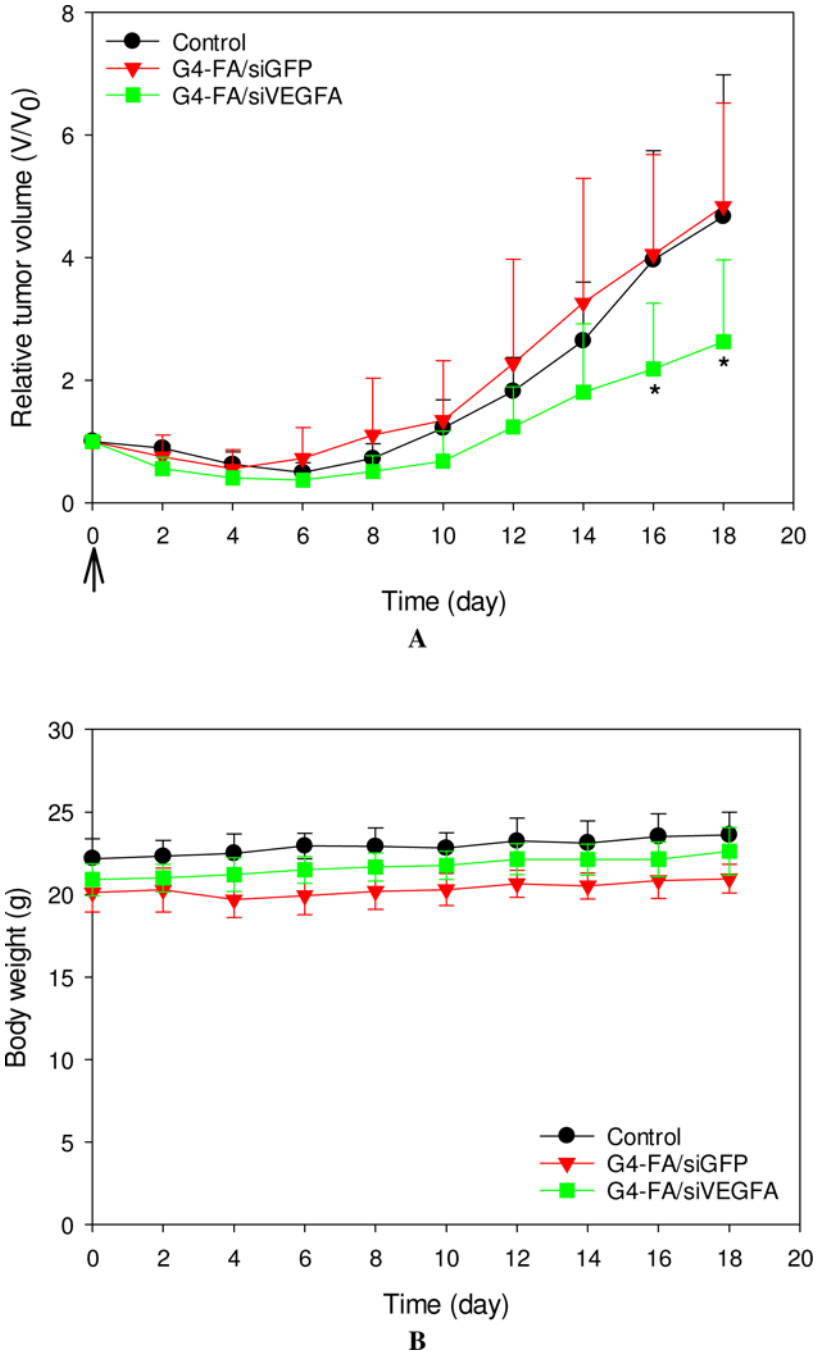

Figure 3.

In vivo assessment of single-dose antitumor effects. HN12 tumor-bearing mice received one dose of PBS (control), G4-FA/siGFP, or G4-FA/siVEGFA at day 0 via i.t. injection, and their tumor volumes (A) and body weights (B) were monitored for 18 days. * $p < 0.05$ versus the control (n = 5). Arrows indicate the day when the mice were inoculated.

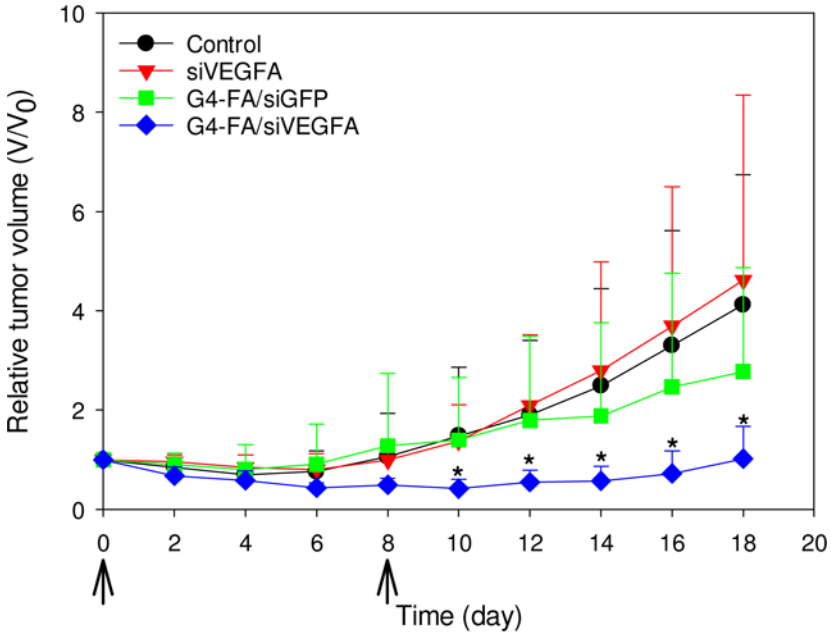

A

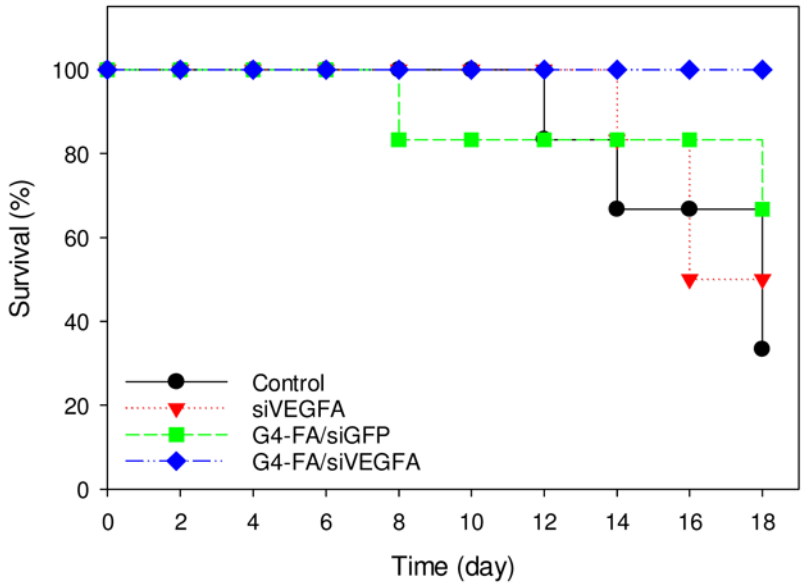

B

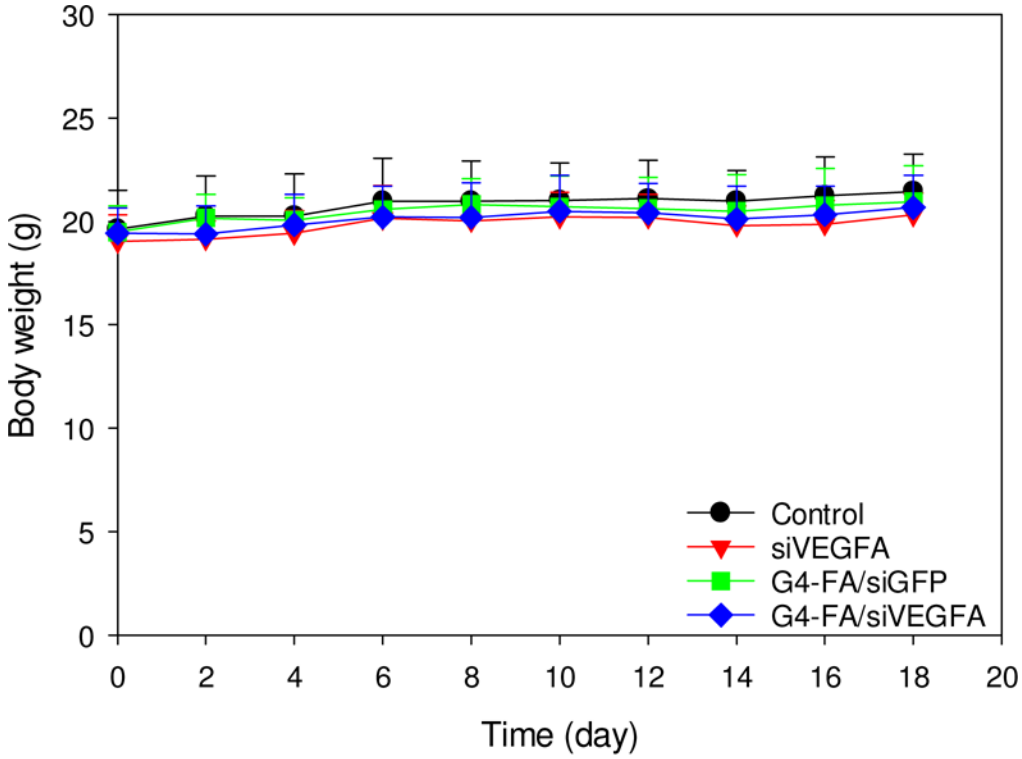

C

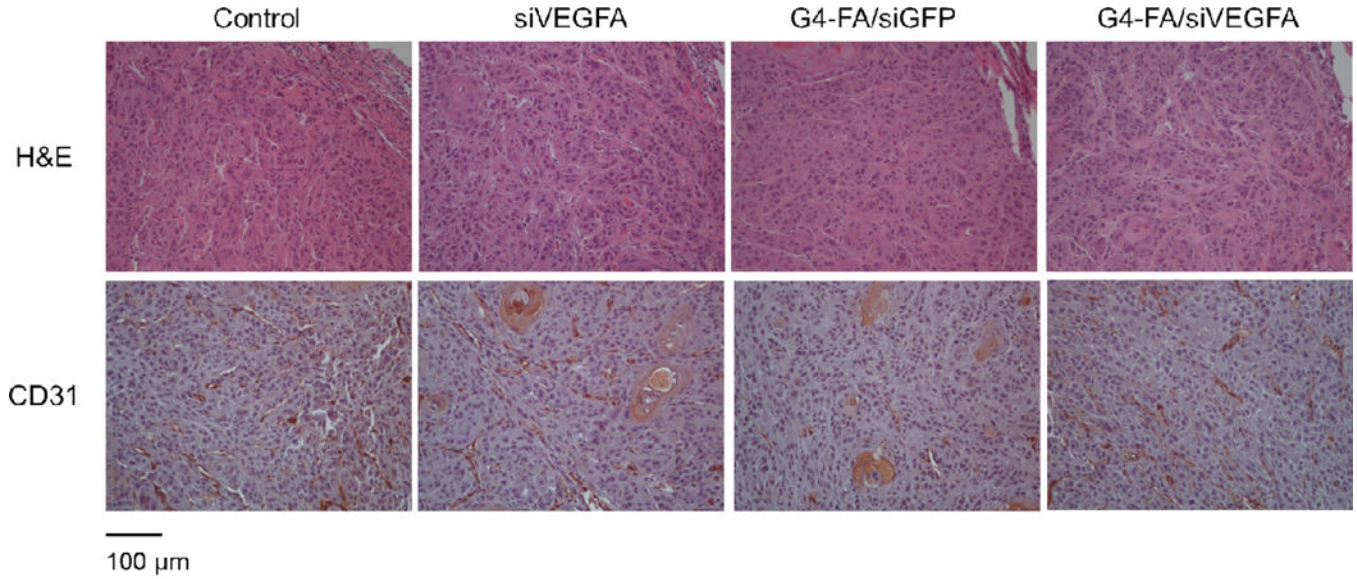

D

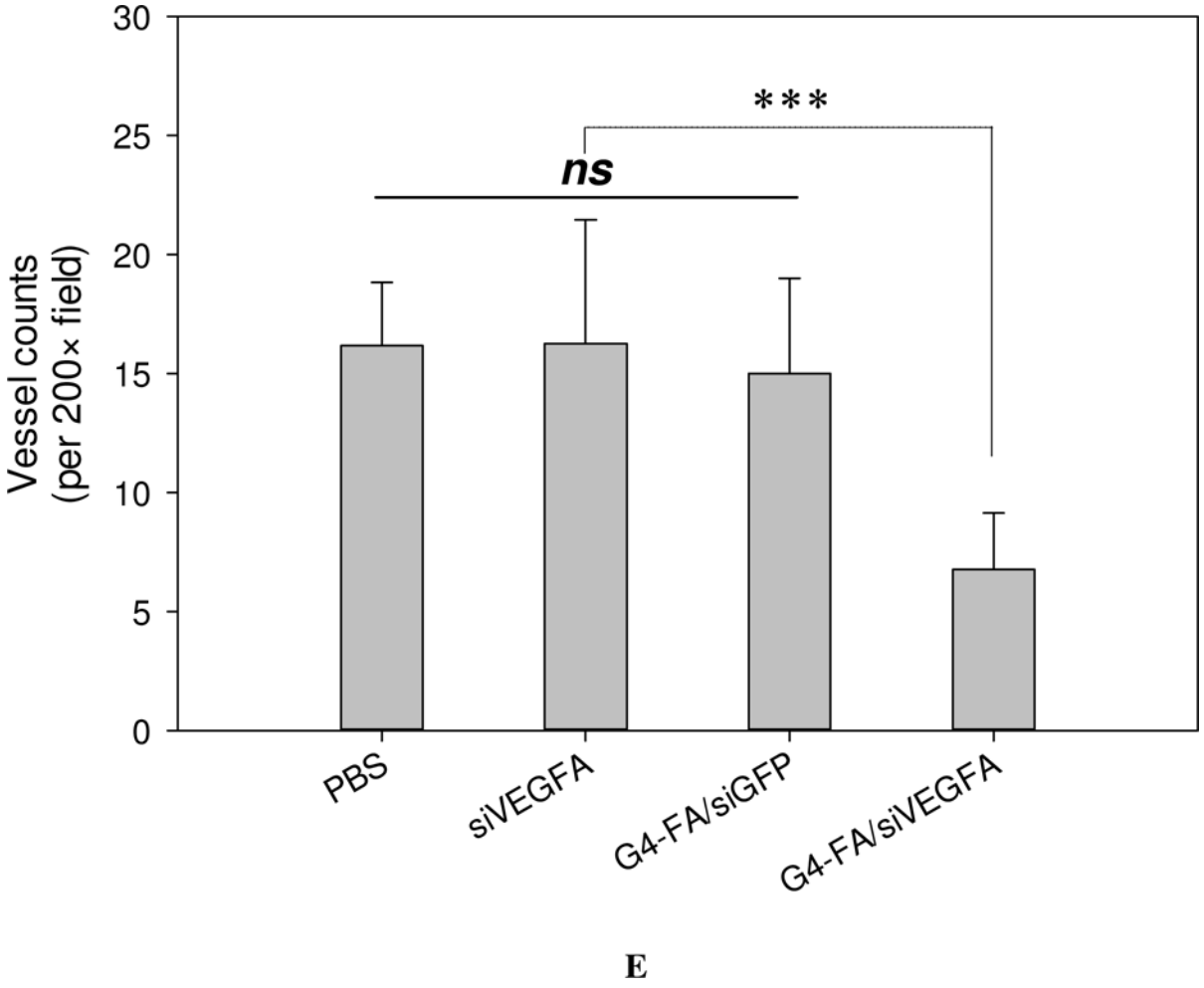

Figure 4.

In vivo assessment of two-dose antitumor effects. HN12-YFP tumor-bearing mice received one dose of PBS, siVEGFA, G4-FA/siGFP, or G4-FA/siVEGFA at day 0 and a second dose at day 8 via i.t. injection. The experiment was terminated at day 18. (A) Tumor volume measured at indicated time points. Arrows indicate the days when the mice were inoculated. * $p < 0.05$ versus the control (n = 6). (B) Kaplan–Meier analysis of mice in all groups using tumor volume 320 mm^3 as a threshold. (C) Body weights of the mice monitored during the experiment. (D) Tumor histology evaluation by H&E tumor staining and CD31 staining. (E) Microvessels (per 200× field) counted as the number of CD31-positive vessels in six randomly selected fields for each treatment. *** $p < 0.001$; ns, not statistically significantly (n=12).

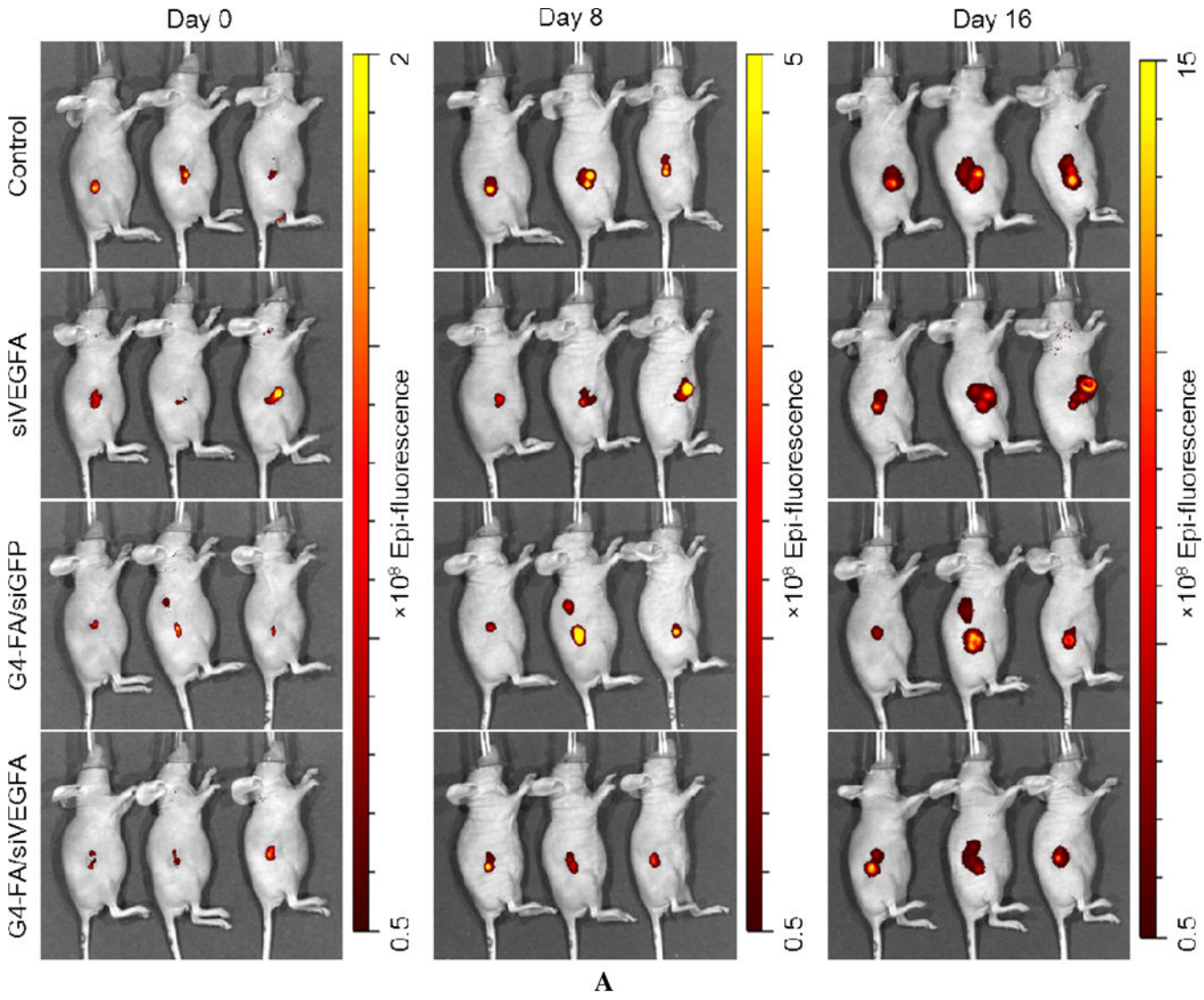

A

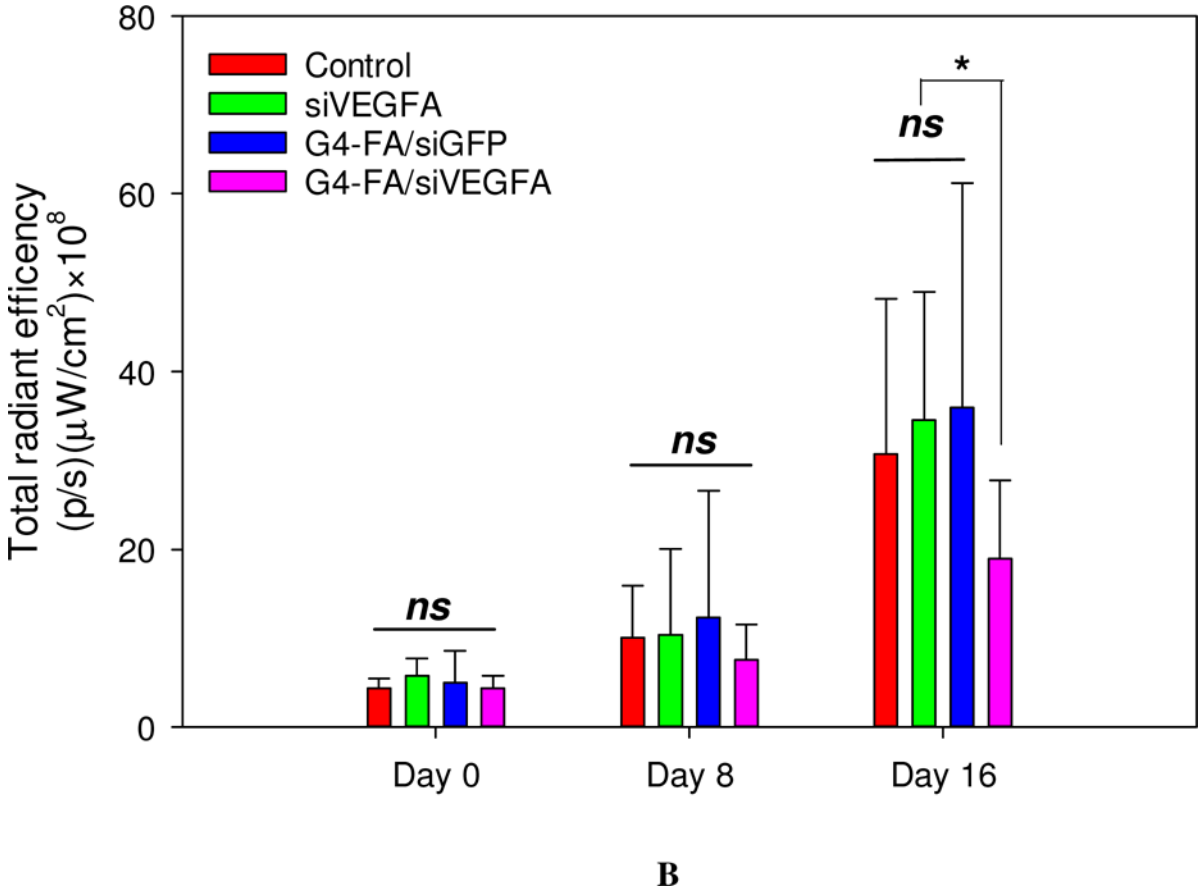

Figure 5.

Semi-quantitative in vivo assessment of two-dose antitumor effects by noninvasive imaging of tumors in the HN12-YFP tumor-bearing mice. (A) Whole-body fluorescence images of the mice in the two-dose experiment at day 0, day 8, and day 16. (B) Quantification of imaging signals, reported as the total radiant efficiency. Total radiant efficiency of tumor was quantified by IVIS based on the images (fluorescence intensity/region of tumor in the image). * $p < 0.05$; ns, not statistically significant (n = 6).

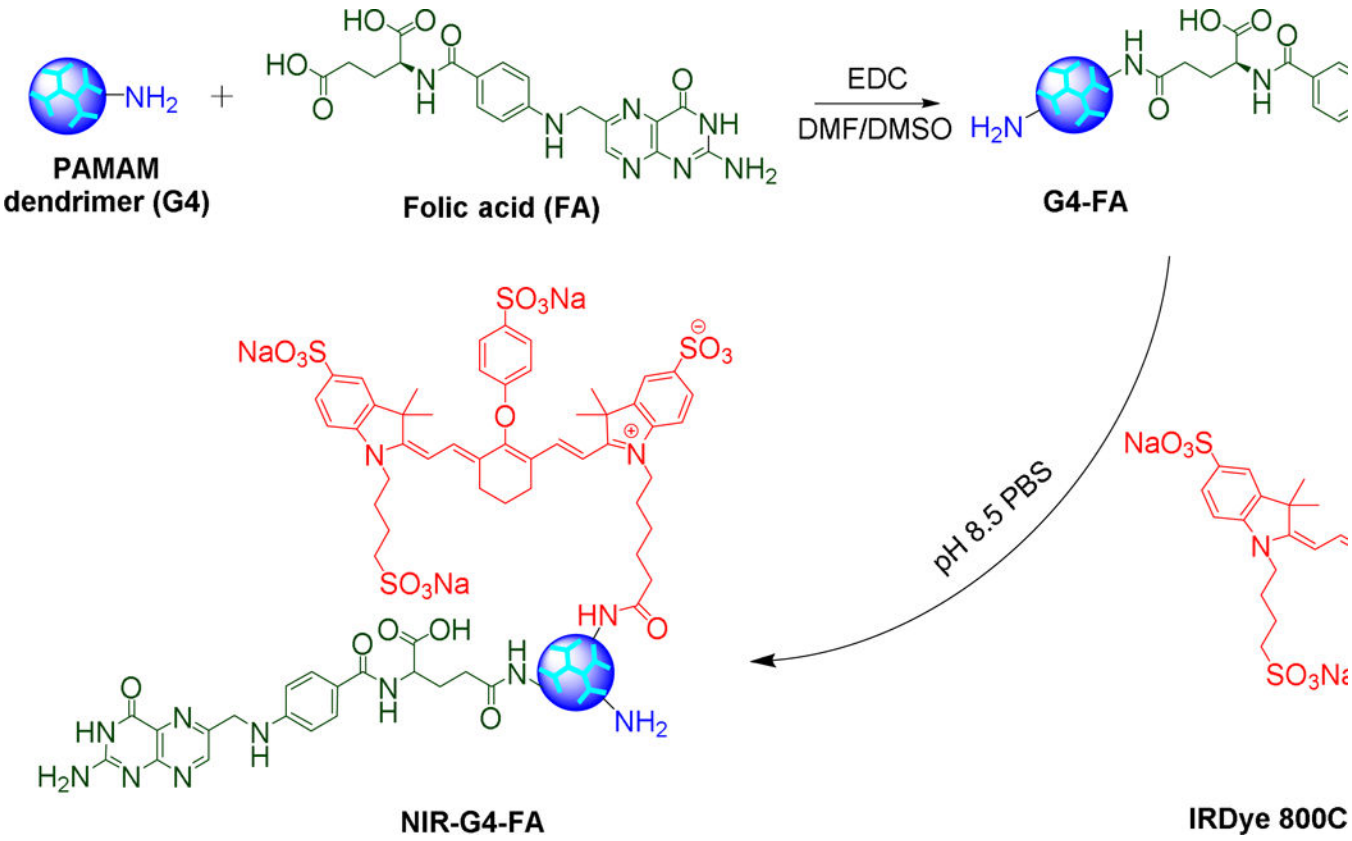

Scheme 1.

Synthesis of folic acid-decorated PAMAM dendrimer G4-FA and near infrared dye labeled G4-FA (NIR-G4-FA).